ELSEVIER

Journal of Nuclear Materials 266–269 (1999) 1145–1150

journal of nuclear materials

Potentials, $\mathbf{E} \times \mathbf{B}$ drifts, and fluctuations in the DIII-D boundary

R.A. Moyer [a,*], R. Lehmer [a], J.A. Boedo [a], J.G. Watkins [b], X. Xu [c], J.R. Myra [d], R. Cohen [c], D.A. D'Ippolito [d], T.W. Petrie [e], M.J. Schaffer [e]

[a] *Fusion Energy Research Program, University of California, San Diego, La Jolla, CA 92093-0417, USA*
[b] *Sandia National Laboratories, Albuquerque, NM 87185, USA*
[c] *Lawrence Livermore National Laboratory, Livermore, CA 94551, USA*
[d] *Lodestar Research Corporation, Boulder, CO 80301, USA*
[e] *General Atomics, P.O. Box 85608, San Diego, CA 92186-5688, USA*

Abstract

Reciprocating Langmuir probes are used to investigate the structure of electrostatic potentials, $\mathbf{E} \times \mathbf{B}$ drifts, and fluctuations in the edge ($\rho < 1$), scrape-off layer (SOL) and divertor of single null diverted discharges in the DIII-D tokamak. These measurements demonstrate that the X-point geometry suppresses potential fluctuations in the drift wave range of frequencies (20 kHz $\leqslant f \leqslant$ 300 kHz) as predicted by theory [N. Mattor and R.N. Cohen, Phys. Plasmas 2 (1995) 4042], and suppresses quasi-coherent modes in the edge of H-modes. Consequently, edge turbulence and ballooning mode stability calculations, such as those used in L–H transition and H mode pedestal theories, must incorporate realistic X-point magnetic geometry to quantitatively reproduce experimental results. In the divertor plasma, root-mean-square potential fluctuations $\tilde{\phi}_{\rm fl}$, are found to be larger in H mode than in L mode, and in detached versus attached divertor plasmas. These measurements have been used to benchmark turbulence simulations with two unique codes that incorporate realistic X-point magnetic geometry: the 3-D boundary turbulence code BOUT and the BAL shooting code with high-n ballooning formalism.

Keywords: Fluctuations; X-point; Plasma edge physics; Scrape-off layer; DIII-D

1. Introduction

Despite several decades of research, our understanding of edge turbulence and transport remains incomplete. For example, the unstable modes, drives and dissipation mechanisms have not yet been conclusively identified [1]. In addition, the effects of conditions such as neutral pressure, radiation, and magnetic shear are not yet completely understood. Significant progress has nonetheless been possible due to the generality of the $\mathbf{E} \times \mathbf{B}$ shear suppression mechanism, which permits turbulent transport to be controlled without the need to identify the underlying modes or drives. Recent theoretical work has focused on the complex issues associated with coupling of the core to the SOL across the H-mode pedestal region, including the effects of neutral pressure [2], neoclassical SOL currents [3], and edge microturbulence [4–7]. Systematic study of the plasma profiles and fluctuations in the boundary is needed to test these increasingly more complex theories.

In this paper, we present measurements of electron pressure $P_{\rm e} = n_{\rm e} K T_{\rm e}$, plasma $\phi_{\rm pl}$ and d.c. floating $\phi_{\rm fl}^{\rm dc}$ potential profiles and potential fluctuations $\tilde{\phi}_{\rm fl}$ at three poloidal locations in the DIII-D tokamak: the outboard midplane, the lower divertor, and the bottom of upper single null discharges – analogous to the 'top' of lower single null divertor plasmas, as shown in Fig. 1. Measurements are obtained with two reciprocating Langmuir probe arrays [8,9] capable of scanning the SOL/

* Corresponding author. Tel.: +1 619 455 2275; fax: +1 619 455 4156; e-mail: moyer@gav.gat.com.

0022-3115/99/$ – see front matter
PII: S0022-3115(98)00618-7

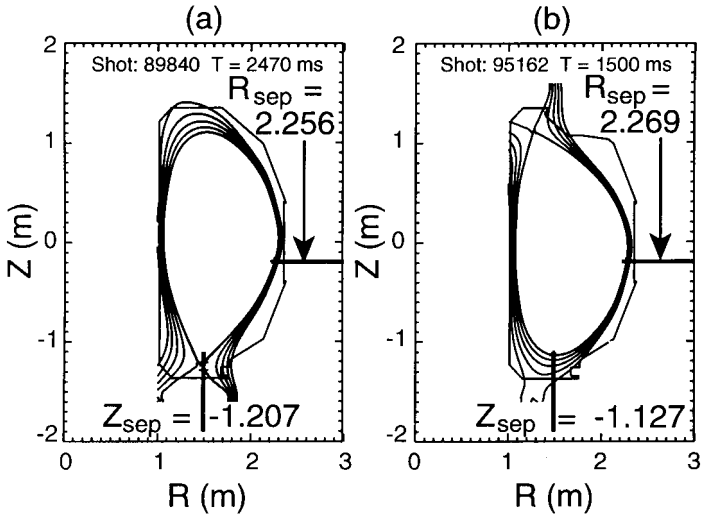

Fig. 1. Equilibrium flux surface reconstructions from EFIT for the (a) lower single null and (b) upper single null divertor discharges in this work. The midplane and X-point probe locations are indicated by the horizontal and vertical bars respectively. The R_{sep} and Z_{sep} values are the locations of the separatrix in the probe path for the midplane probe ($Z_{probe} = -0.19$ m) and X-point probe ($R_{probe} = 1.488$ m) respectively.

divertor plasma up to and just inside the separatrix. The probe array in the lower divertor, the 'X-point probe', provides simultaneous measurements of n_e and T_e, the main ion flows parallel to the magnetic field [10], and the d.c. and fluctuating floating potential ϕ_{fl}^{dc} and $\tilde{\phi}_{fl}$. These measurements are compared with the same quantities measured simultaneously at the outboard midplane and with the results of simulations using the BOUT 3-D boundary turbulence code [11] and of calculations using the BAL shooting code with high-n ballooning formalism [12]. These codes have the unique capability to handle realistic X-point magnetic geometry, which is critical for reproducing the experimental results.

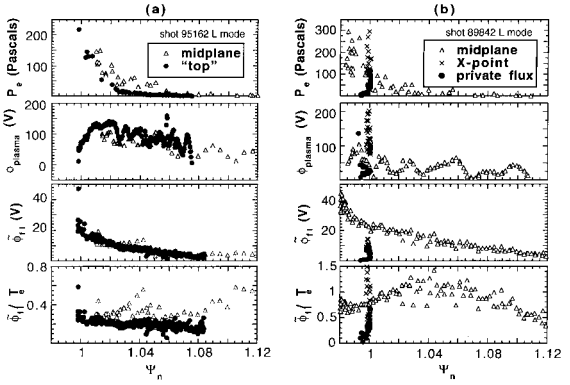

Fig. 2. Profiles of local plasma and potential fluctuation parameters versus normalized poloidal flux coordinate Ψ_n for L mode discharges with (a) upper single null and (b) lower single null divertors. In (a) the X-point probe scans a region equivalent to the 'top' (•) of a lower single null discharge. In (b) the X-point probe scans the lower divertor private flux (•) and the outer SOL and X-point (×) regions. The profiles are, from top to bottom: electron pressure P_e, plasma potential ϕ_{pl}, absolute rms potential fluctuation level $\tilde{\phi}_{fl}$, and normalized rms potential fluctuation level $\tilde{\phi}/T_e$.

2. Poloidal variation of potential fluctuations

Data have been acquired in two sets of single null divertor L mode discharges: lower and upper single null. Significant changes to the inside of the DIII-D vessel, including installation of the upper outer divertor baffle plate and cryopump [13], occurred between the time that the lower and upper single null data were acquired. To account for these variations, the data from the lower divertor chamber are compared against simultaneous outboard midplane measurements in each case. Typical measurements in the SOL at the 'top' of the discharge (a) and in the vicinity of the X-point (b) are shown in Fig. 2. In Fig. 2(a), the electron pressure P_e profile at the 'top' (•) is similar in shape to the midplane profile (Δ), indicating that P_e is nearly poloidally symmetric, to within the uncertainty in the flux surface mapping. Both the plasma potential ϕ_{pl} and the rms potential fluctuation amplitude $\tilde{\phi}_{fl}$ map well from the 'top' to the outboard midplane. T_e profile differences lead to a reduction in the normalized rms amplitude from 30% on the outboard midplane to 20% at the 'top'. For the set of discharges in Fig. 2(b), the X-point was located just inboard of the vertical stroke of the X-point probe, pro-

viding access to the X-point vicinity but limiting the amount of data obtained in the outer SOL [Fig. 1(a)]. The data in the outer SOL and plasma core (×) near the X-point cover a limited range in the normalized poloidal flux coordinate Ψ_n: $0.998 \leqslant \Psi_n \leqslant 1.002$, although the spatial extent is 5 cm (outer SOL) and 4 cm (core); see Fig. 5. Near the X-point, the local P_e and ϕ_{pl} have strong poloidal variations which complicate comparisons with the midplane measurements. However, it is clear that: (1) P_e near the X-point exceeds the midplane value, (2) a strong gradient in ϕ_{pl} exists across the separatrix between the private flux and SOL regions [14], and (3) the rms amplitude $\tilde{\phi}_{fl}$ is a factor of 2 or more lower near the X-point than on the same Ψ_n surface at the outboard midplane.

These conclusions are confirmed by analysis of the potential fluctuations at a fixed Ψ_n in the frequency domain, as shown in Fig. 3. In Fig. 3(a), the potential autopower spectrum $P_{\phi\phi}(\omega)$ (proportional to $\tilde{\phi}_{fl}^2$) at the "top" of the plasma near the separatrix ($\Psi_n = 1.01$ corresponding to 0.5 cm outside the separatrix on the outboard midplane) is comparable to the midplane spectrum across the frequency range associated with the turbulent particle transport $\Gamma(\omega)$. In contrast, $P_{\phi\phi}(\omega)$ near the X-point [Fig. 3(b)] is substantially reduced in the frequency range $20 \leqslant f \leqslant 300$ kHz where most of the turbulent particle transport $\Gamma(\omega)$ occurs. Similar results are obtained up to $\Psi_n = 1.01$ into the SOL (2 cm in effective midplane radius). Together, these measurements indicate that electrostatic fluctuations due to $\mathbf{E} \times \mathbf{B}$ drift wave like modes in the frequency range 20 kHz $\leqslant f \leqslant$ 300 kHz are suppressed in the vicinity of the X-point, as predicted by Mattor et al. [15].

In Fig. 4(a), $P_{\phi\phi}(\omega)$ on the outboard midplane is compared to $P_{\phi\phi}(\omega)$ near the X-point in a ELM-free H-mode phase. The L-mode spectrum is also shown for reference. These spectra show that the rms amplitude $\tilde{\phi}_{fl}$ obtained by integrating $P_{\phi\phi}(\omega)$ over ω is larger near the X-point in H-mode than in L-mode due to an increase in $P_{\phi\phi}(\omega)$ in the drift wave range of frequencies that were strongly suppressed in L-mode. However, $P_{\phi\phi}(\omega)$ at the X-point remains lower than the midplane value in the drift wave range of frequencies due to the lack of strong quasi-coherent mode activity which is seen just inside the separatrix at the midplane in these H-modes. In Fig. 4(b), the autocorrelation functions corresponding to the H-mode midplane and X-point power spectra in Fig. 4(a) are compared. The midplane potential autocorrelation function shows a clear signature of strong coherent activity (the periodic oscillations in the wings of the autocorrelation function), while this feature is far less pronounced (but not completely absent) in the X-point data. These measurements indicate the quasi-coherent mode, which dominates the potential (and density, not shown here) power spectra at the midplane, is also greatly suppressed near the X-point.

3. Divertor potentials and fluctuations: L versus H mode

Although it is common to measure fluctuation suppression right after the L–H transition, fluctuations can

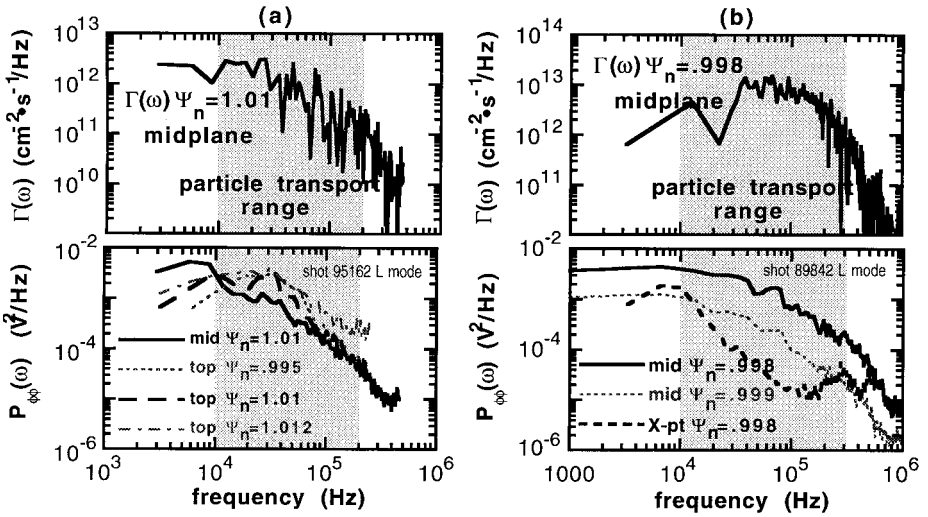

Fig. 3. Comparison of potential fluctuation autopower spectra $P_{\phi\phi}(\omega)$ for (a) the 'top' and midplane at $\Psi_n = 1.01$, and (b) the X-point vicinity and midplane at $\Psi_n = 0.998$ in single null divertor L mode discharges. The frequency resolved turbulent particle flux $\Gamma(\omega)$ is shown to indicate the frequency range where most of the particle transport is driven (shaded regions). Due to uncertainties in mapping the data to a common Ψ_n value, power spectra from neighboring Ψ_n (a) at the 'top' of the machine and (b) at the outboard midplane are provided to demonstrate that the conclusions are insensitive to the mapping uncertainties.

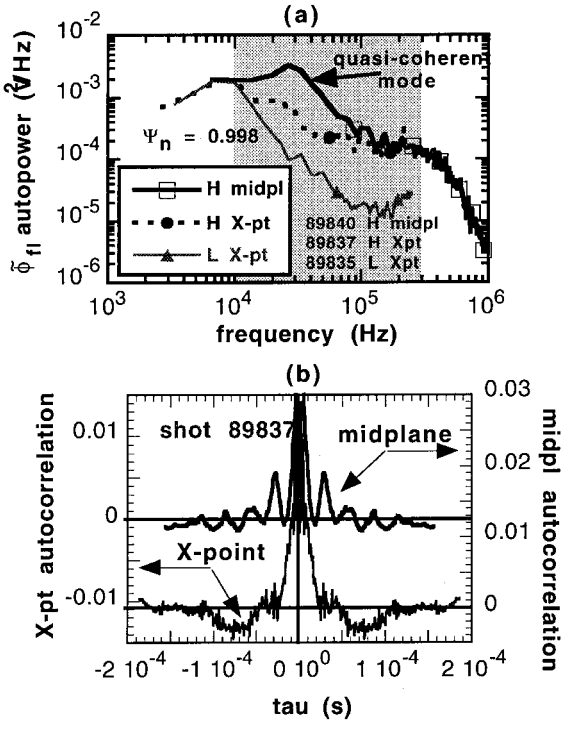

Fig. 4. (a) Comparison of potential fluctuation autopower spectra $P_{\phi\phi}(\omega)$ near the X-point (•) and at the outboard midplane (□) in an ELM-free H-mode. The L mode $P_{\phi\phi}(\omega)$ (▲) is shown for comparison. The frequency range for turbulent particle transport is shaded. (b) Comparison of the potential autocorrelation functions near the X-point and on the outboard midplane. The data for (a) and (b) are both from $\Psi_n = 0.998$.

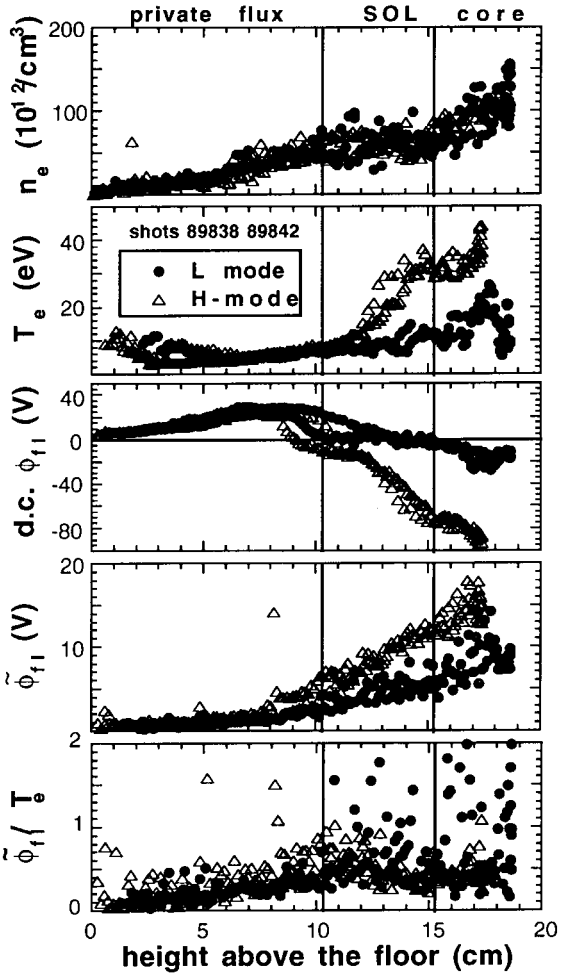

Fig. 5. Variation of plasma and potential fluctuation parameters versus height above the divertor target in established (•) L and (△) ELM-free H-mode phases of identical discharges in DIII-D. The regions where the X-point probe is traversing the private flux, outer SOL, and core regions are indicated. The parameters are, from top to bottom: electron density n_e, electron temperature T_e, d.c. floating potential ϕ_{fl}^{dc}, absolute rms potential fluctuation level $\tilde{\phi}_{fl}$, and normalized rms potential fluctuation level $\tilde{\phi}/T_e$.

rise inside the E_r shear layer/H-mode pedestal region in established H-modes due to increased turbulence drive, particularly for potential fluctuations [16]. In Fig. 5, changes in the vicinity of the X-point between established L and ELM-free H-modes (just prior to ELM onset) are shown. Although the local density is essentially unchanged, T_e rises significantly in both the outer SOL and in the core near the X-point. There is a corresponding drop to a more negative ϕ_{fl}^{dc}. The rms potential fluctuations $\tilde{\phi}_{fl}^{dc}$, however, are a factor of 2 higher across the outer leg of the divertor and into the core near the X-point in H-mode. This measurement contrasts with measurements at the outboard midplane, where the electrostatic fluctuation amplitudes are higher only inside the separatrix, not in the SOL [16]. The result is that the normalized rms amplitude remains nearly constant, although there is considerably more 'jitter' at low frequency [$f \leqslant 10$ kHz; Fig. 4(a)] in the L-mode phase. This jitter may be related to the fact that most low power L-modes, like those reported here, are either partially or fully detached in DIII-D.

4. Potentials and flucutations in detached divertor plasmas

In Fig. 6(a), we compare the divertor conditions for attached (•) and detached (△), slowly ELMing H-mode discharges. For these probe plunges, the outer strike point was over the penetration in the divertor floor for the probe, and the probe traveled nearly within a flux surface, yielding profiles that rise rapidly to the maximum value and remain nearly constant thereafter. Consistent with detachment, n_e is 2–4× higher and T_e 2–3× lower in the outer leg of the divertor. Note that in detached plasmas, the swept double probe yields values

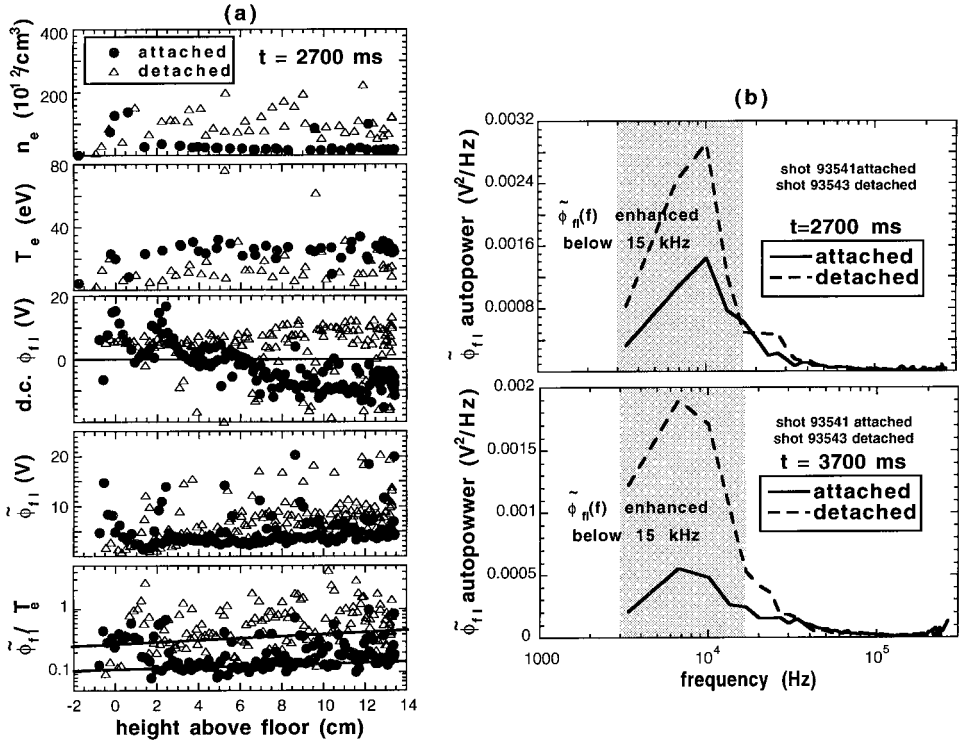

Fig. 6. (a) Variation of plasma and potential fluctuation parameters versus height above the divertor target in established, slowly ELMing H-modes with (•) attached and (Δ) detached outer divertor leg plasmas. The parameters are, from top to bottom: electron density n_e, electron temperature T_e, d.c. floating potential ϕ_{fl}^{dc}, absolute rms potential fluctuation level $\tilde{\phi}_{fl}$, and normalized rms potential fluctuation level $\tilde{\phi}/T_e$. Note the logorithmic y axis for the plot $\tilde{\phi}/T_e$. (b) Potential fluctuation autopower spectra $P_{\phi\phi}(\omega)$ in slowly ELMing (top; $t = 2700$ ms) and rapidly ELMing (bottom; $t = 3700$ ms) with (solid) attached and (dashed) detached outer divertor leg plasmas. The region below about 16 kHz where $P_{\phi\phi}(\omega)$ is strongly enhanced during detachment is indicated by the shaded areas.

for T_e that are systematically 2–3 times higher than T_e from divertor Thomson scattering [17] so that the values of $\tilde{\phi}/T_e$ reported here for detached plasmas are lower bounds. This difference arises primarily due to the distortion of the probe I–V characteristics by the large amplitude, low frequency (1 kHz $\leqslant f \leqslant$ 15 kHz) fluctuations [10] which are strongly enhanced in detached divertor plasmas, as shown in Fig. 6(b). Note also that attached plasmas generally have $\phi_{fl}^{dc} < 0$ [Fig. 5(a); Fig. 6(a)]. When the divertor detaches, the floating potential rises above 0, but is transiently carried negative during each ELM. This behavior suggests that some ELMs transiently reattach the divertor plasma. It was previously reported [17] that ELMs transiently enhanced $\tilde{\phi}/T_e$ by a factor of 2 in attached divertors, and a factor of 2–10 in detached divertors. In Fig. 6(a), it is clear that the rms amplitude $\tilde{\phi}_{fl}$ is increased a factor of 2 in detachment even between the slow ELMs. Combined with the decrease in T_e, this leads to an increase in the normalized amplitude $\tilde{\phi}/T_e$ by a factor 2–4 between ELMs, and much more during the ELMs [note the logorithmic scale in Fig. 6(a)]. Later in these discharges, the neutral beam power was increased to produce rapidly ELMing H-modes. Similar results were obtained in those rapidly ELMing phases.

5. Discussion

The data presented here have been used to 'benchmark' simulations of the boundary (edge and SOL) turbulence [11] with the BOUT code [18]. The BOUT code simulates $\mathbf{E} \times \mathbf{B}$ drift resistive ballooning-like modes in realistic DIII-D magnetic geometry. The code has, for turbulence codes, the unique ability to model the X-point geometry properly. For the discharges presented here, the BOUT code calculates that the broadband turbulence is due to drift resistive ballooning-like modes with toroidal mode number n between 200 and 400. The resulting density fluctuation power spectra and frequency resolved particle flux $\Gamma(\omega)$ are qualitatively consistent with the spectra measured at the outboard midplane, including a significant range of f^{-1} dependence [11]. The BOUT simulations also show that the

unstable modes associated with the turbulence do not extend into the X-point region, consistent with the experimental data.

Myra et al. have modeled the appearance of a strong quasi-coherent feature in the ELM-free H-mode with BAL, a shooting code with high-n ballooning formalism [12], which also incorporates the X-point magnetic geometry. Using the high-n ballooning formalism, the code finds modes that are robustly unstable for $n < 50$ and are near the ideal MHD stability boundary. The code yields instability for this class of modes only in the H-phase of the discharge. The corresponding eigenmodes balloon in the bad curvature region and are small in the X-point and divertor region [19]. These calculations are consistent with the experimental observations in Section 2.

Watkins et al. have determined that the probability distribution for T_e at the target plates in detached divertor plasmas is strongly skewed from a low of 1–2 eV to 10 eV due to the presence of energetic electrons in the pulse associated with the ELM [20]. Such an energetic (nonthermal) electron pulse would effect on the floating potential measurements, driving the d.c. potential negative as observed during the ELMs. While this observaton explains the large excursions in ϕ_{fl}^{dc} and $\tilde{\phi}/T_e$ during the ELMs, it does not explain the large normalized fluctuation amplitudes $\tilde{\phi}/T_e$ in L-mode and between ELMs in detached H-mode conditions. In these detached divertor plasmas, the X-point region is dynamically very active, appearing to "flicker" between a detached state and an attached state spontaneously triggered by the ELM heat and/or energetic electron pulses burning through the radiating zone.

6. Summary

Electrostatic fluctuations in the DIII-D boundary are found to be suppressed in the vicinity of the X-point relative to both the outboard midplane and the 'top' of the SOL. Strong quasi-coherent mode activity inside the separatrix in H-modes (inside the E_r shear layer) is also strongly suppressed near the X-point. These observations are consistent with modeling of the broadband turbulence (BOUT) and the quasi-coherent modes (BAL) in the full X-point geometry. These results stress the importance of incorporating realistic magnetic geometry into turbulence and MHD stability codes such as those routinely used to evaluate L–H transition models [7].

The rms fluctuation amplitude $\tilde{\phi}_{fl}$ in the divertor increases in H mode relative to L mode due to a broadening of the fluctuation power spectrum. The spectral broadening raises the mean frequency above the 5–10 kHz typically seen in L mode divertor plasmas to values closer to those at the midplane and top of the SOL. The low mean frequency and narrow power spectra in L mode are similar to those in detached, ELMing H-mode discharges, most likely due to the tendency of low power L modes like those studied here to be partially or fully detached in DIII-D. The low frequency fluctuations lie outside the frequency range of $\mathbf{E} \times \mathbf{B}$ drift wave-like modes where most of the anomolous perpendicular transport occurs, and are quite different in character from broadband turbulence (e.g. $\tilde{\phi}/T_e$ and $\tilde{\phi}/\phi > 1$). The data present a picture of the X-point region of detached diverted discharges as dynamically very active, in contrast to having a well-defined "equilibrium" about which there are relatively small turbulent oscillations.

Acknowledgements

Work supported by US Department of Energy under Grant DE-FG03-95ER54294, and Contract Nos. DE-AC03-89ER51114, W-7405-ENG-48, DE-FG02-97ER54392 and DE-AC04-95AL85000.

References

[1] B.A. Carreras, IEEE Trans. on Plasma Science 25 (1997) 1281.
[2] L.W. Owen et al., Plasma Phys. Control Fusion 40 (1998) 717.
[3] F.L. Hinton, G.M. Staebler, Nucl. Fusion 29 (1989) 405.
[4] J.G. Cordey, W. Kerner, O. Pogutse, Plasma Phys. Control. Fusion 37 (1995) 773.
[5] R.H. Cohen, X.Q. Xu, Phys. Plasmas 2 (1995) 3374.
[6] J.G. Cordey et al., Plasma Phys. Control. Fusion 38 (1996) 1905.
[7] B. Rogers, J.F. Drake, Phys. Rev. Lett., submitted.
[8] J.G. Watkins et al., Rev. Sci. Instrum. 63 (1992) 4728.
[9] J.G. Watkins et al., Rev. Sci. Instrum. 68 (1996) 373.
[10] J.A. Boedo et al., these Proceedings.
[11] X.Q. Xu et al., these Proceedings.
[12] J.R. Myra, D.A. D'Ippolito, J.P. Goedbloed, Phys. Plasmas 4 (1997) 1330.
[13] S.L. Allen et al., these proceedings.
[14] J.A. Boedo et al., Plasma Flow in the DIII-D Divertor in 25th European Physical Society Conference on Controlled Fusion and Plasma Physics 1998, European Physical Society, Czech Republic, Prague.
[15] N. Mattor, R.N. Cohen, Phys. Plasmas 2 (1995) 4042.
[16] R.A. Moyer et al., Phy. Plasmas 2 (1995) 2397.
[17] R.A. Moyer et al., J. Nucl. Mater. 241-243 (1996) 633.
[18] X.Q. Xu, R.H. Cohen, Contributions to Plasma Physics 36 (1996) 202.
[19] J.R. Myra et al., In 1998 International Sherwood Theory Conference 1998, Atlanta, Georgia.
[20] J.G. Watkins et al., these Proceedings.